

Contents lists available at ScienceDirect

Journal of Physics and Chemistry of Solids

journal homepage: www.elsevier.com/locate/jpcs





Electronic structure and chemical bonding in transition-metal-mixed gallium oxide (Ga₂O₃) compounds

C.V. Ramana ^{a,*}, Swadipta Roy ^{a,b}, Vishal Zade ^a, Anil K. Battu ^{a,b}, Nanthakishore Makeswaran ^a, V. Shutthanandan ^b

- a Center for Advanced Materials Research (CMR), University of Texas at El Paso, 500 W University Ave., El Paso, TX, 79968, USA
- ^b Environmental Molecular Sciences Laboratory (EMSL), Pacific Northwest National Laboratory (PNNL), Richland, WA, 99352, USA

ARTICLE INFO

Keywords: $\beta\text{-Ga}_2O_3$ Doping Ga_2O_3 composites Electronic properties

ABSTRACT

Transition metal (TM)-mixed gallium oxide (Ga_2O_3) ceramic compounds have potential applications in optical, optoelectronic, and photovoltaic devices. Herein, we report on the salient electronic structures and chemical properties of a series of such compounds, with a view to optimizing performance. The TM-mixed Ga_2O_3 ($Ga_2 \times M_xO_3$; TM-GO; $0.0 \le x \le 0.3$, $0.0 \le x \le$

1. Introduction

Gallium oxide (Ga_2O_3), which is emerging as a novel material in modern electronics and optoelectronics, continues to attract scientific and research interest [1–10]. This significant interest in Ga_2O_3 and related materials is primarily due to their unique properties and phenomena, which can be readily exploited in many of the modern optical, electronic, optoelectronic, photocatalytic, and energy storage and conversion device technologies [1–15].

From crystal-structure and solid-state functional material perspectives, Ga_2O_3 is an interesting candidate material for applications, since it exhibits polymorphism depending on the thermodynamic conditions employed during its synthesis and/or operation [16–18]. Distinct α , β , γ , δ , and ε phases of Ga_2O_3 are known, as reported in the literature [16–21]. Among these known polymorphs, β - Ga_2O_3 exhibits exceptional chemical and thermal stability [1,3,21–23]. At ca. 4.8 eV, β - Ga_2O_3 exhibits the second widest band gap of any material (after diamond), coupled with a high dielectric breakdown voltage of 8 MV [1,24,25].

These unique physical, chemical, optical, electronic, and optoelectronic properties make intrinsic and doped $\beta\text{-}Ga_2O_3\text{-}based$ materials interesting for various technological applications, particularly in solar-blind ultraviolet (UV) photodetectors [6,7], photocatalysis [5,14,15], high-power electronic devices [1,24], light-emitting diodes [5], transparent conducting oxides (TCOs) [26], lithium-ion batteries [8], and integrated chemical sensors [9,22,23]. However, in all the aforementioned applications, fundamental understanding of the crystal structure, morphology, electronic structure, optical and electrical properties and, most importantly, the structure–property relationships, is key to achieving enhanced device performance and efficiency when utilizing Ga_2O_3 and other Ga-oxide-based materials.

In view of the aforementioned technological applications, and also to derive new functionalities or enhanced performance, doping or alloying of $\beta\text{-}Ga_2O_3$ with transition metal (TM) or rare-earth (RE) ions has been gaining tremendous importance in recent years [3,5,10,26–39]. Improving luminescence and electroluminescence and related properties has been the primary focus for doping $\beta\text{-}Ga_2O_3$ with RE ions [5,27,

E-mail address: rvchintalapalle@utep.edu (C.V. Ramana).

^{*} Corresponding author.

28]. Similarly, attention directed towards the use of TM ions to dope β-Ga₂O₃ has been particularly to engineer optical, electrical, or optoelectronic properties and device efficiencies [3,10,29-40]. In the context of either RE or TM ion-doping, a brief introduction to the crystal structure and related aspects of β-Ga₂O₃ is reasonable to understand the effects of specific dopants and their intrinsic nature on the structure, properties, and phenomena of the resulting compounds. β-Ga₂O₃ crystallizes in a base-centered monoclinic (space group C2/m) crystal structure with lattice parameters of a = 12.214, b = 3.0371, c = 5.7981Å, and $\beta=103.83^\circ$ [41,42]. In the monoclinic unit cell, Ga is either tetrahedrally or octahedrally coordinated by oxygen atoms. On the other hand, oxygen atoms occupy three different lattice sites in a distorted cubic close-packed arrangement around the Ga sites [20,41]. Thus, manipulation of the structure and/or defects by introducing suitable dopants into β-Ga₂O₃ permits engineering of the structure and properties to meet the requirements of a given technological application.

In view of the technological importance of β-Ga₂O₃ and Ga-oxidebased alloys and compounds, there have been numerous experimental and theoretical studies on the effects of doping [3,5,10,26-39]. For instance, Si-doping of β-Ga₂O₃ enables control of its electrical conductivity [33]. Villora et al. demonstrated enhanced n-type conductivity in Si-doped β-Ga₂O₃ compared to undoped Ga₂O₃, which they ascribed to the introduction of Si⁴⁺ at Ga sites creating electron donors [33]. Tunable electrical characteristics, namely carrier density and electrical resistivity, have been demonstrated in Sn-doped Ga₂O₃ single crystals [26]. Density functional theory (DFT) calculations on doped β-Ga₂O₃ have provided theoretical insights into the effects of various metal ion dopants on its electronic structure and properties [31,32]. Based on the DFT calculations, it was reported that W, Mo, and Re act as deep donors, whereas Nb, with its lower formation energy, acts as a shallow donor [31]. Some studies have concerned aspects of the doping of β-Ga₂O₃ in the form of thin films [10,35,36,38-40]. For example, the optical band gap of β-Ga₂O₃ polycrystalline thin films was found to be narrowed by doping with Cu [10,35], Nb [36], W [39], and Ti [40], although the reduction in the band gap depends on the dopant concentration and chemistry of the materials [38-40,43]. However, there have only been a few limited studies that demonstrate or interlink the electronic structure with band-gap engineering of Ga₂O₃ through doping so as to produce materials suitable for integration into optical devices with a spectral selectivity across a broader range of the electromagnetic spectrum. Specifically, there have been very few studies on understanding the electronic structure and chemical bonding changes in TM-doped and/or mixed Ga₂O₃ (TM-GO), which may be intimately connected with the overall optical, electrical, and optoelectronic properties of the doped Ga₂O₃ bulk ceramic system. This is the primary objective and focus of the present work.

The present work is directed towards a fundamental scientific understanding of the electronic properties of TM-mixed Ga₂O₃ (Ga_{2-x}M_xO₃, denoted as TM-GO) compounds. Specifically, efforts have been made to study the effects of Fe-, Ti-, and W-mixing of Ga_2O_3 and to derive a comprehensive fundamental scientific understanding of the electronic structures of the resulting compounds. These TM ions are interesting to produce mixed oxides or doped compounds of Ga oxide and to correlate the properties. In addition, the respective oxides of these TM ions, i.e., Fe₂O₃, WO₃, and TiO₂, are known to exhibit excellent and/or comparable photocatalytic activity, generating a considerable charge carrier concentration for an interesting set of possible electronic applications [44-50]. Moreover, like Ga₂O₃, the oxides of Fe, W, and Ti are well known to exhibit interesting electronic properties, and have demonstrated potential in the design and development of sensors and photo-detectors [44-50]. In our previous research, we directed our efforts towards elucidating the fundamental science of doped Ga2O3 materials, especially the design and development of materials with controlled chemical, physical, structural, and optical properties [3,13, 26,29,30,38-40,43,44,51]. We paid utmost attention to tailoring of the optical band gap in thin films synthesized by sputter deposition,

whereby the deposition temperature and/or doping method for different dopant concentrations are the variables [13,39,40]. Additionally, we have continued to investigate the effect of TM ion alloying and doping in Ga₂O₃ ceramics, whereby the objective is to elucidate the fundamental science and mechanistic aspects of metal-doping on the structure and properties. In this context, solid-state synthesis and detailed structural characterization of Fe-doped Ga₂O₃ have revealed the effect of Fe³⁺ substitution of Ga³⁺ in octahedral and tetrahedral coordination environments, which is possible because of their similar Shannon ionic radii [29]. Correlations between chemical composition, crystal structure, and dielectric properties have also been established [29]. In addition, electrocatalytic activity has been demonstrated for Fe-doped Ga₂O₃, whereas no such activity is observed for undoped Ga₂O₃ [43]. Detailed investigations on Ti-doped Ga₂O₃ ceramic materials synthesized by high-temperature solid-state chemical reaction have indicated that single-phase compounds are only formed at very low levels of Ti doping (<5 at.%) [26]. Higher Ti-doping levels result in composite formation with an undissolved TiO2 phase [26]. Moreover, Ti-doping induces abnormal grain growth and lattice-twinning-induced striations compared to undoped Ga₂O₃ [26]. Electrocatalytic studies have indicated that Ti-doped Ga₂O₃ compounds exhibit appreciable activity, whereas undoped Ga₂O₃ does not [26]. We have also observed some interesting effects of W-doping in Ga₂O₃ [3]. Synthesis and structural characterization of W-doped Ga₂O₃ (GWO) revealed the formation of a clear solid solution at low W-doping levels ($x \le 0.10$), whereas an unreacted WO₃ secondary phase separated at x>0.10. Therefore, in view of the observed differences in crystal structures, phases, and morphologies, it was deemed useful to compare and contrast dopant effects in TM-GO from the fundamental perspective of electronic properties.

In the context of doped, alloyed, or mixed oxides based on Ga₂O₃, the relevance and consideration of the TM-GO system and specific TM ions for incorporation into Ga₂O₃ in this work is due to the following reasons. It was deemed interesting to compare and contrast the behavior of the compounds obtained by doping Ga₂O₃ with Fe, Ti, or W due to the fact that their chemical valence states and electronegativities are different. Although other chemical valence states are possible, under normal conditions, the most stable configurations of these dopants are Fe³⁺, Ti⁴⁺, and W⁶⁺, respectively. Moreover, these Fe, Ti, and W ions have different Shannon ionic radii compared to that of Ga³⁺ in Ga₂O₃. Given that the optical, electrical, and optoelectronic properties of doped Ga₂O₃ are mostly determined by the overall electronic structure and properties, deriving a fundamental scientific understanding and comparison of the effects of different TM ions in Ga₂O₃ is highly pertinent. Understanding the effects of various TM ions with variable chemistry and physics may provide fundamental insight in a broader context, and the implications derived may apply to a large class of doped compounds or other similar materials. Furthermore, Ti and W have been proposed as metal contacts for Ga₂O₃ for use in power electronic devices [1,24]. Therefore, fundamental understanding of the doping effects of the set of TM ions considered in this work could be useful in predicting the surface/interface diffusion and reaction products (if any) in device applications involving such TM-Ga₂O₃ heterostructures and contacts. These hybrid oxides are mainly prepared by a powder metallurgy route involving a solid-state reaction. This kind of synthesis does not produce compact structures, and the problem of porosity of the compounds often arises. These defect structures are responsible for interface diffusion, as elaborated by Shirsath et al. [52]. Furthermore, the demonstrated approach based on interface engineering to realize the potential of multilayered oxides for novel ferroelectric states and functionalities clearly paves the way for studies of other hybrid or mixed oxides for developing highly efficient, environmentally friendly, and highly scalable solid-state electronic devices [52]. Additionally, the proposed TM-GO compounds and ceramic materials with controlled structure and properties may also be useful as target materials for high-quality thin-film deposition by physical vapor deposition methods. Therefore, in this work, TM-GO compounds were produced using a simple, versatile, high-temperature

solid-state chemical reaction method. The electronic properties of the resulting compounds have been studied as a function of variable TM content as well as TM ions with different chemistries. The results obtained are presented and discussed in this paper.

2. Experimental details

2.1. Synthesis

The conventional solid-state reaction method was employed to synthesize the transition metal (TM)-mixed Ga₂O₃ compounds (Ga_{2-x}M_xO₃; abbreviated as "TM-GO"). In order to better understand the effect of TMdoping and to compare the effects of various metals, samples with similar contents (x values) of the various dopants in Ga₂O₃ were prepared. Specifically, the TM concentration in TM-GO was varied in the range x = 0.0–0.3. We adopted previously established procedures and methods [3,26,29,30,43] to synthesize TM-doped Ga₂O₃ compounds with the aim of performing a detailed comparative study of their electronic structures, surface chemistry, and electrocatalytic activities. The synthesis procedures and mixtures were adapted to ensure charge balance in the compounds with respect to the dopant ions. The dopants considered were Fe, Ti, and W. High-purity metal oxide powder precursors, namely Ga₂O₃ (99.99%), Fe₂O₃ (99.9%), TiO₂ (99.9%), and WO₃ (99.9%), were employed to produce the respective TM-GO (TM = Fe, Ti, W) compounds [3,26,29,30]. The procured high-purity precursors of Ga₂O₃ and the respective metal oxide (Fe₂O₃/TiO₂/WO₃) were weighed in stoichiometric proportions with respect to the desired composition. The weighed powders were combined in an agate mortar and pulverized using acetone as the wetting medium to obtain homogeneously mixed TM-GO compounds. GFO, GWO, and GTO were pelletized at 1200 °C for 6 h, 1250 °C for 6 h, and 1350 °C for 8 h, respectively. The phase purity was ascertained by X-ray diffraction (XRD) analysis with reference to previous work. Phase purity was only attained at low TM-doping levels; a secondary phase of undissolved TM oxide separated at higher dopant levels [3,26]. Furthermore, as we have reported previously, increasing the sintering temperature modified the effective densities of the compounds [3,26,29,30]. The integration and annexation of smaller grains are the main reasons for the decrease in porosity, which eventually leads to continuous grain growth. As the sintering temperature is increased, the grains acquire enormous kinetic energy for grain boundary movement in the form of thermal energy and ultimately smaller grains coalescence to form larger grains [3,26,29]. Previous efforts directed at Fe-, Ti-, and W-doped Ga₂O₃ compounds clearly indicated that the final sintering temperature must be adjusted depending on the melting points of the respective TM oxides in order to ensure homogeneous mixtures [3,26,29]. This was taken into consideration in the synthesis of the respective TM-GO ceramics. Also, although it is not relevant in the context of electronic structure and chemical bonding studies as presented and discussed in this paper, electrical conductivity studies of the samples indicated that TM incorporation effectively decreases the electrical resistivity [29]. This is attributed to electron hopping between the various cations. The following specific synthetic conditions were adopted to produce the respective TM-GO compounds.

2.1.1. Iron (Fe)-Mixed Ga₂O₃

The synthesis of Fe-mixed Ga_2O_3 ceramic compounds by the high-temperature solid-state chemical reaction method has been described elsewhere [29,43]. Fe-mixed Ga_2O_3 samples were prepared by homogeneously mixing the precursors and then calcining them at $1100\,^{\circ}\text{C}$ for 6 h. The heating and cooling rates of the muffle furnace were both set at $10\,^{\circ}\text{C/min}$. Calcined powders were ground in order to break down large lumps into fine particles of size around $50\text{--}70\,\mu\text{m}$. The main purpose of grinding was to ensure a uniform particle size distribution for better pelletization. A uniaxial hydraulic press was used to cast pellets (8 mm diameter, 2 mm thickness) at an applied load of 5 ton. These pellets were

then sintered at $1200\,^{\circ}$ C for 6 h for densification. As reported elsewhere, the optimum conditions resulted in effective densification of the GFO compounds, with their relative porosity decreasing to around 10%, as well as a uniform distribution of grains [29].

2.1.2. Titanium (Ti)-Mixed Ga₂O₃

The synthesis of Ti-mixed Ga_2O_3 compounds by the high-temperature solid-state chemical reaction method has been described elsewhere [26]. After careful weighing of the precursors in stoichiometric proportions, they were thoroughly mixed in an agate mortar. Acetone was used as a wetting medium to facilitate the process. Pulverization was followed by calcination at 1250 °C for 12 h, which involved intermittent grinding to reduce stresses in the powder. The phase purity of the powder was confirmed prior to pelletization at a higher temperature. Poly vinyl alcohol (PVA) was added to each sample, and they were ground to ensure proper dispersion [26]. These powders were then pressed into pellets of diameter 8 mm and thickness 1 mm using a uniaxial hydraulic press (MTI Corporation, Richmond, CA, USA) at 1.5 ton. These pellets were then sintered at 1350 °C for 8 h [26].

2.1.3. Tungsten (W)-Mixed Ga₂O₃

The synthesis of W-mixed Ga_2O_3 compounds by the high-temperature solid-state chemical reaction method has been described elsewhere [3,30]. The process entails homogenization of WO_3 and Ga_2O_3 powders followed by calcination at $1050\,^{\circ}\text{C}$ for $12\,\text{h}$ and then at $1150\,^{\circ}\text{C}$ for $12\,\text{h}$. The entire process was carried out in a muffle furnace, with intermittent grinding of the mixture to ensure complete reaction. Sinterability was further enhanced by grinding the calcined powder to reduce its size. PVA binding agent was added prior to pelletization of the calcined powder. Disc-shaped pellets of diameter 8 mm and thickness 1 mm were pressed using a uniaxial hydraulic press with a load of 1.5 ton. These pellets are known as green pellets; they were heated at $5\,^{\circ}\text{C}/\text{min}$, held at $500\,^{\circ}\text{C}$ for $30\,$ min for binder burnout, and finally sintered at $1250\,^{\circ}\text{C}$ for $6\,\text{h}$ [3,30].

2.2. Characterization

2.2.1. X-ray photoelectron spectroscopy (XPS)

X-ray photoelectron spectroscopic (XPS) scans of the TM-GO ceramic compounds were obtained with a Kratos Axis Ultra DLD spectrometer equipped with an Al- K_{α} monochromatic X-ray source (1486.6 eV) and a high-resolution hemispherical analyzer [26,30,43]. We adopted previously established procedures and methods for XPS characterization of undoped and doped Ga₂O₃ materials [26,30]. For full disclosure, the details of XPS measurements and analytical procedures are given here. The X-ray source was set at an output power of 105 W and the emitted photoelectrons were collected by the detector, which was placed normal with respect to the sample. The sample size area was restricted to 700 \times $300 \, \mu m^2$, and the pass energy was set at 160 eV for survey scans and 20 eV for high-resolution scans. The step sizes were 0.5 eV and 0.1 eV for survey and high-resolution scans, respectively. After setting these initial parameters, calibration was performed with a standard Ag sample (FWHM of 0.59 eV for the Ag $3d_{5/2}$ core level). Since these are insulating ceramic oxide samples, charge neutralization was set at 4.2 eV when securing the samples on the stub with Cu tape. After completion of the experiment, data analysis was carried out with CasaXPS software with Gaussian/Lorentzian GL (30) line shape with line asymmetry and Shirley background correction.

The above procedure was employed due to its efficacy in evaluating the undoped and doped Ga_2O_3 compounds [26,30]. Survey scans were performed over a binding energy (BE) range of 1400 eV, and high-resolution spectra were obtained from at least 16 sweeps for each element. The objective is a well-defined peak [26,30]. To avoid the interference of the Ga 3d peak by the O 2s peak, only Ga 2p spectra were considered. The sample surface was cleaned with ozone cleaner for 5 min to eliminate any hydrocarbon contamination. The C 1s peak at

284.8 eV was used as a reference for all scans [26,30].

3. Results and discussion

XPS survey spectra of the TM-GO compounds with x=0.1 and x=0.2 are compared in Fig. 1a and b, respectively. Characteristic XPS peaks due to Ga and O are seen for all of the samples, along with peaks due to the respective dopants (Fe, Ti, and W). The presence of a C 1s peak in the spectra is due to adventitious carbon, which arises due to air exposure between synthesis and placing the samples in the XPS system [26,30]. Therefore, the spectra were calibrated to this C 1s peak at a BE of 284.8 eV. This is part of our sample analysis, and has proved to be useful for undoped and doped Ga_2O_3 compounds in our previous work [26,30]. Electronic structures and chemical compositions were further probed by means of detailed high-resolution core-level XPS scans of Ga, O, Fe, Ti, and W. Being a surface-sensitive characterization technique, XPS allowed us to understand the surface chemistry of the TM-GO compounds and the chemical valence state(s) of the constituent elements, as discussed below.

The XPS core-level spectra of the Ga 2p region are presented in Fig. 2. For comparison, the Ga 2p core-level scans obtained for undoped and TM-doped Ga₂O₃ compounds are presented together. Fig. 2a shows the Ga 2p core-level XPS patterns of the TM-GO (TM = Fe, Ti, and W) compounds with x = 0.1, and Fig. 2b shows the corresponding patterns for samples with x = 0.2. The Ga 2p region features the expected Ga 2p doublet of Ga 2p_{3/2} and Ga 2p_{1/2} peaks at BEs of 1117.5 and 1144.2 eV, respectively. The Ga 2p_{3/2} component is located at a BE of 1116.7 eV for Ga metal [51,53]. Thus, the Ga 2p_{3/2} peak shows a positive BE shift with respect to that of Ga metal, indicating that Ga ions exist in their higher valence state in all of the TM-GO ceramic compounds [53,54]. The positive shift in the BE of the Ga 2p_{3/2} peak is due to a redistribution of the electronic charge [53–55]. No changes in BE and/or peak shape were observed for the Ga 2p region as a function of Fe-, Ti-, or W-doping in the

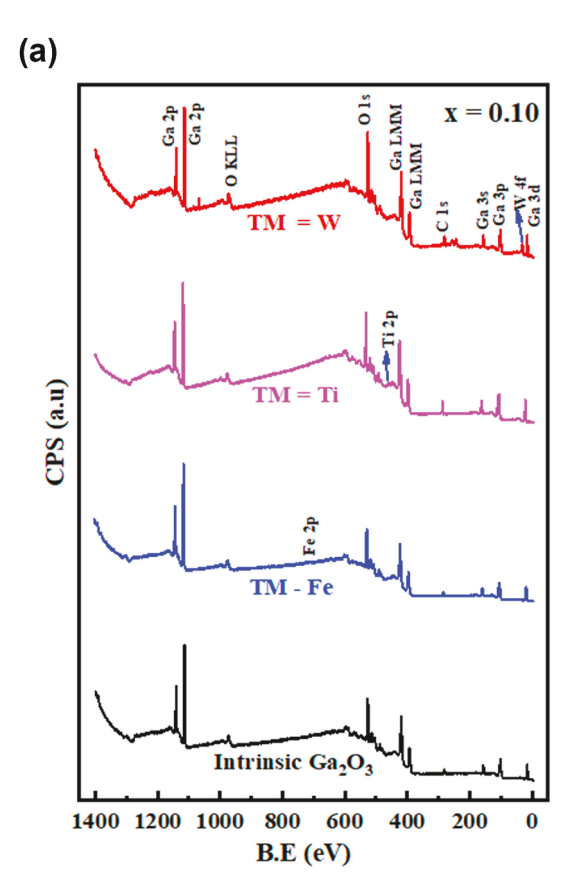


Fig. 1a. XPS survey scans of TM-GO (TM = Fe, Ti, W; x = 0.1) compounds.

(b)

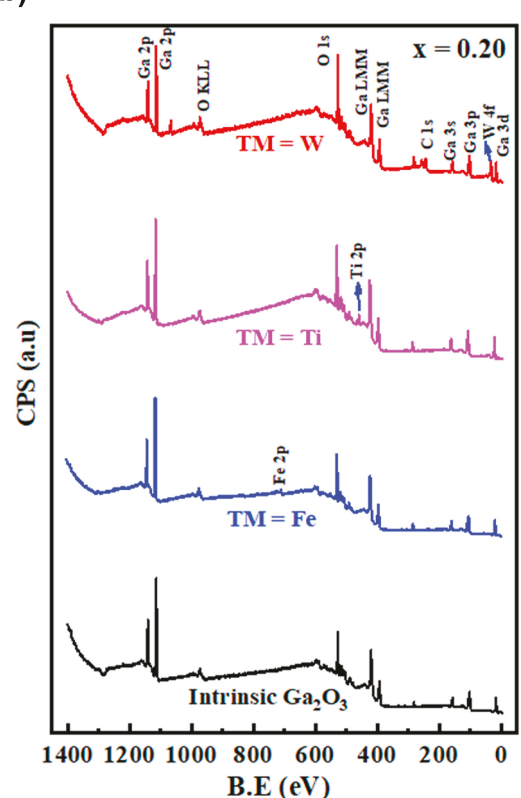


Fig. 1b. XPS survey scans of TM-GO (TM = Fe, Ti, W; x = 0.2) compounds with higher dopant concentration.

TM-GO compounds, remaining consistent with reported values for ${\rm Ga_2O_3}$ in the literature [51,54]. This reiterates that all of the Ga ions were present in the highest valence state (${\rm Ga^{3^+}}$) in all of the TM-GO compounds, irrespective of the nature of the TM-ion. Comparison of the Ga 2p core-level XPS data of the TM-GO (TM = Fe, Ti, and W) compounds with higher dopant concentration (x=0.2; Fig. 2b) indicates a similar result. It can be seen that, even with increasing TM content, the Ga 2p doublet comprising the Ga $2p_{3/2}$ and Ga $2p_{1/2}$ peaks remains located at the same BE and exhibits similar features as noted for the TM-GO (TM = Fe, Ti, and W) compounds with x=0.1. Thus, analysis of the Ga 2p core-level XPS data for various TM-doped ${\rm Ga_2O_3}$ compounds and as a function of dopant concentration (x) clearly indicates that the Ga ion chemical state is unaffected by any of these dopants and is invariably ${\rm Ga^{3^+}}$.

High-resolution XPS patterns for O 1s in the TM-doped Ga₂O₃ ceramic compounds are presented in Figs. 3 and 4. For comparison and clarity of presentation, the XPS data for O 1s obtained for both undoped and TM-doped Ga₂O₃ compounds with variable dopant concentrations are shown. Fig. 3 shows the O 1s core-level XPS patterns of the TM-GO (M = Fe, Ti, and W) compounds with x = 0.1. It is evident that, for all of the synthesized TM-doped Ga₂O₃ compounds, as well as for undoped Ga₂O₃, the O 1s peak is not symmetric. The asymmetric O 1s peak can be resolved into two component regions: (i) an intense main peak centered at BE \approx 530.7 eV, and (ii) two small shoulder peaks located at higher BEs of 532.2 and 533.4 eV. These three component peaks indicate three different chemical states or chemical bonding environments around oxygen [56,57] in the TM-GO ceramic compounds. The main O 1s peak component corresponds to oxygen bonded to gallium (Ga-O bonds) [53, 54,58-60], as expected for stoichiometric Ga₂O₃. It has been reported in the literature that the O 1s peak for stoichiometric undoped Ga₂O₃ generally occurs at BE \approx 530.5–531.0 eV [53,58–60]. Comparison of the O 1s peak data (Table 1) indicates that this peak remains at a

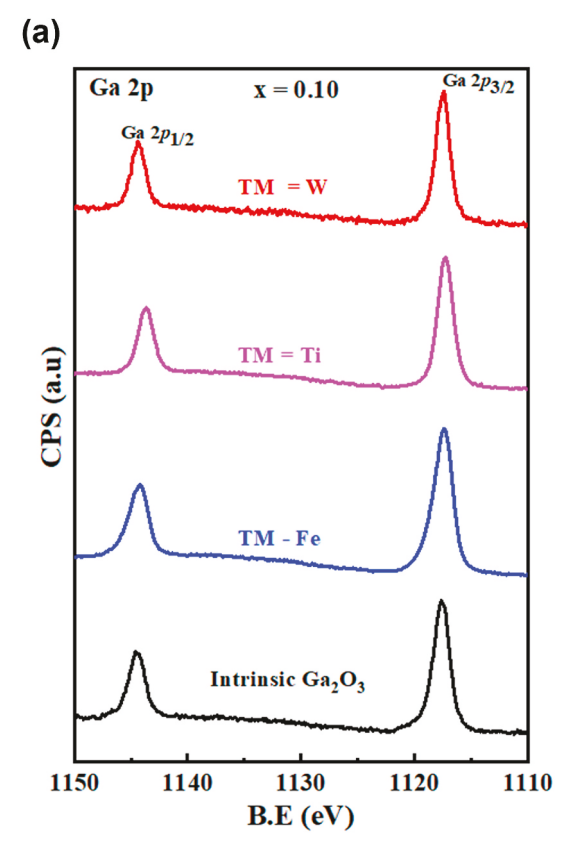


Fig. 2a. Ga 2p core-level XPS patterns of TM-GO (TM = Fe, Ti, W; x=0.1) compounds. Comparison of the data for the intrinsic and TM-doped $\rm Ga_2O_3$ compounds reveals no significant changes in the Ga 2p peak components.

well-defined BE. The data confirm the persistence of Ga–O bonds, which are a signature of stoichiometric Ga_2O_3 , in all of the TM-GO compounds. The shoulder peaks at BEs of 532.2 and 533.4 eV can be attributed to surface oxygen bound to carbon in the form of either carbonyl (oxygen bonded to carbon, C–O) or hydroxyl (oxygen bonded to hydrogen, O–H) groups [56,57]. These functional chemical groups may be adsorbed on the sample surface as impurities during sample transfer from the fabrication chamber and/or furnace atmosphere to the XPS load lock [53,56,57]. Thus, their appearance as shoulder contributions with minor intensities is justified, as encountered in many of our previous studies on different oxide samples [30,38,40,53].

Fig. 4 shows the high-resolution XPS patterns for O 1s in the TM-GO (TM = Fe, Ti, and W) compounds with higher dopant concentration (x = 0.2). The O 1s peak data for the TM-GO compounds are presented in Table 2. As described for x = 0.1, the O 1s peaks are also seen to be asymmetric at x = 0.2. Deconvolution of the peak results in components, of which that with major intensity is characteristic of Ga–O bonds in Ga₂O₃. Comparison of the data for undoped Ga₂O₃ and TM-GO compounds with x = 0.1 and 0.2 clearly indicates that the characteristic Ga–O bonds of Ga₂O₃ persist throughout the TM-GO compounds (Table 3). Similarly, the shoulder peaks corresponding to the surface C–O or C–O–H bonds are seen for all of the compositions.

High-resolution core-level XPS patterns of Fe-, Ti-, and W-mixed samples are shown in Figs. 5 and 6. Fig. 5 shows the Fe 2p, Ti 2p, and W 4f core-level XPS patterns of the TM-GO (TM = Fe, Ti, and W) compounds with x=0.1. Similarly, Fig. 6 shows the Fe 2p, Ti 2p, and W 4f core-level XPS patterns of the TM-GO compounds with x=0.2. The high-resolution XPS scan of the Fe 2p region [Fig. 5 (a) and 6 (a)] presents interesting features revealing the characteristics of Fe bonding and chemical state in Ga_2O_3 , especially as a function of variable Fe content (x). The characteristic doublet of Fe 2p, that is, Fe $2\text{p}_{3/2}$ and Fe $2\text{p}_{1/2}$

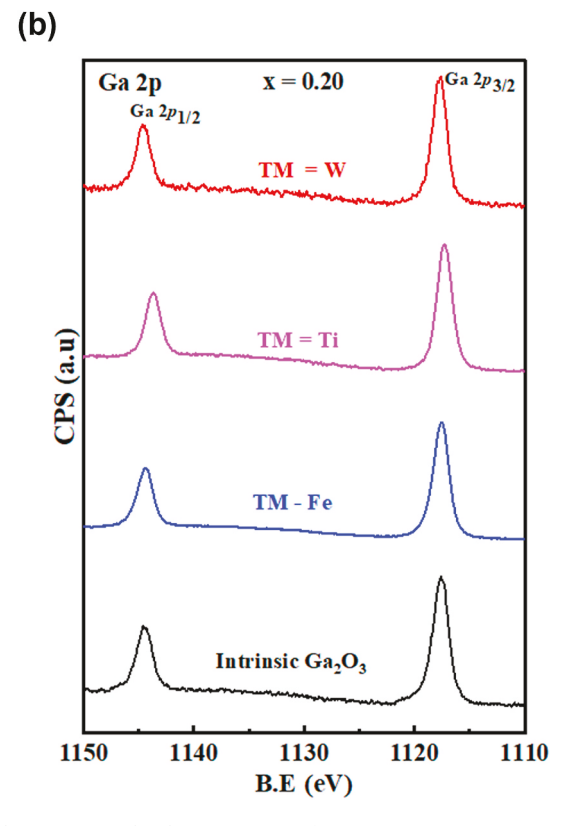


Fig. 2b. Ga 2p core-level XPS patterns of TM-GO (M = Fe, Ti, W; x=0.2) compounds with a higher dopant concentration. Comparison of the data for the intrinsic and TM-doped $\rm Ga_2O_3$ compounds reveals no significant changes in the Ga 2p peak components.

peaks, due to spin-orbit splitting [60,61], can be seen for all of the TM-GO compounds. However, the evolution of these peaks, in terms of shape, etc., is different, and informative about the chemical state and bonding environment of Fe in Ga₂O₃. The BEs of the Fe 2p_{3/2} and Fe $2p_{1/2}$ peaks are presented in Tables 1 and 2 for x = 0.1 and 0.2, respectively. At the lower dopant level (x = 0.1), the Fe $2p_{3/2}$ peak exhibits a highly asymmetric shape [Fig. 5 (a)], indicating the presence of Fe ions in multiple chemical/oxidation states, as well as satellite peaks [61-69]. In addition, for the 2p_{3/2} peak, a shake-up satellite peak is noted at a BE of ca. 720 eV. Peak-fitting analysis and the resulting deconvoluted spectrum of the Fe 2p_{3/2} peak [Fig. 5 (a)] clearly reveals the two principal components with major and minor intensities, respectively. The BE position of the major intensity component of the Fe 2p_{3/2} peak at ca. 711 eV characterizes the existence of Fe in its highest chemical valence state (Fe³⁺), while the other component with a minor intensity corresponds to Fe in its lower valence state (Fe²⁺) [66–68]. There have been numerous literature reports of the BEs of Fe 2p_{3/2} core-level XPS peaks depending on the oxidation or chemical state of the Fe ions [61-69]. For metallic iron (Fe), the reported BE values of the Fe $2p_{3/2}$ core-level peak are in the range 706.7–707.4 eV [66–69]. It can be noted that this is not at all the case in the present work, and the formation of metallic Fe states can be completely ruled out in Fe-doped Ga₂O₃. For Fe-containing compounds, especially oxides, the chemical bonding environment around Fe changes the overall electronic charge distribution, resulting in a BE shift for Fe 2p3/2 to higher energy. The reported BEs of Fe $2p_{3/2}$ for iron existing in the Fe²⁺ chemical state are in the range 709.3-710.0 eV [63,66-69], and those for iron existing in the Fe³⁺ chemical state are in the range 710.6–711.5 eV [63–69]. Furthermore, for the Fe²⁺ and Fe³⁺ chemical states, such as in FeO and Fe₂O₃, respectively, the Fe 2p_{3/2} core-level XPS peak is characterized by the presence of a shake-up satellite [63,64,69]. These satellite peaks often

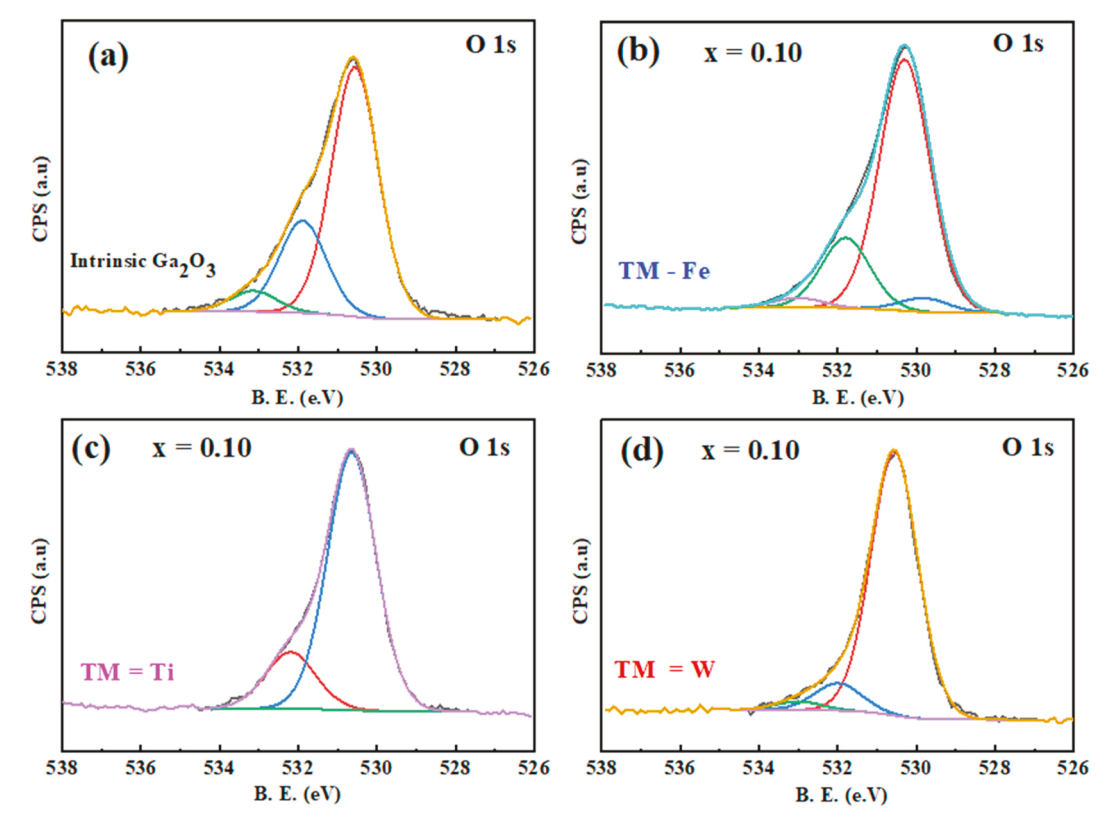


Fig. 3. O 1s core-level XPS patterns for TM-GO (TM = Fe, Ti, W; x = 0.1) compounds.

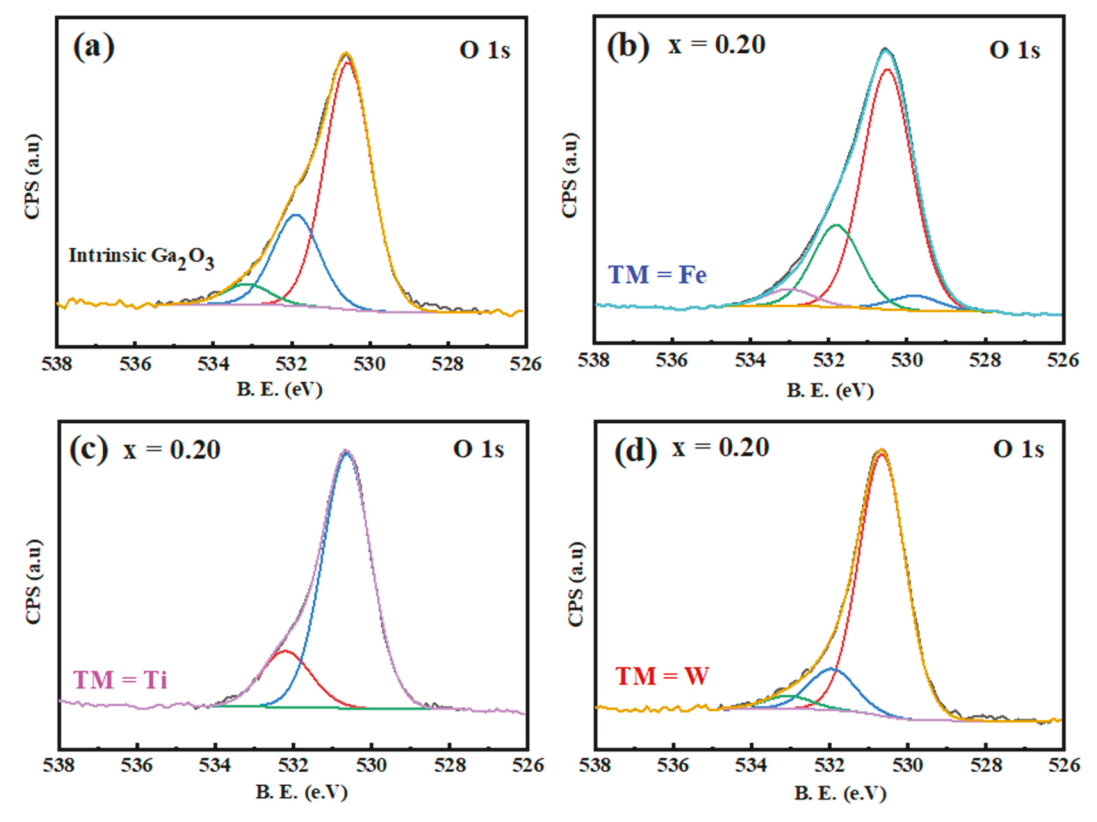


Fig. 4. O 1s core-level XPS patterns of TM-GO (TM = Fe, Ti, W; x = 0.2) compounds with higher dopant contents.

Table 1 XPS peak positions of Ga 2p, O 1s, Fe 2p, and W 4f core-level components in TM-GO (TM = Fe, Ti, W; x = 0.1) compounds. The BE values of Ga $2p_{1/2}$, Ga $2p_{3/2}$, O 1s, Fe $2p_{1/2}$, Fe $2p_{3/2}$, Ti $2p_{1/2}$, Ti $2p_{3/2}$, W $4f_{5/2}$ and W $4f_{7/2}$ are presented.

Compound	XPS Peak Positions (Binding Energy, eV)									
	Ga 2p _{1/2}	Ga 2p _{3/2}	O 1s	Fe 2p _{1/2}	Fe 2p _{3/2}	Ti 2p _{1/2}	Ti 2p _{3/2}	W 4f _{5/2}	W 4f _{7/2}	
Intrinsic Ga ₂ O ₃	1144.49	1117.52	530.61	_	_	_	_	_	_	
Fe-doped Ga ₂ O ₃	1144.21	1117.36	530.25	711.04	724.30	_	_	_	_	
Ti-doped Ga ₂ O ₃	1143.73	1117.25	530.63	_	_	458.74	463.88	_	_	
W-doped Ga ₂ O ₃	1144.37	1117.44	530.59	_	_	-	_	37.56	35.45	

Table 2 XPS peak positions of Ga 2p, O 1s, Fe 2p, and W 4f core-level components in TM-GO (TM = Fe, Ti, W; x = 0.2) compounds. The BE values of Ga $2p_{1/2}$, Ga $2p_{3/2}$, O 1s, Fe $2p_{1/2}$, Fe $2p_{3/2}$, Ti $2p_{3/2}$, Ti $2p_{3/2}$, W $4f_{5/2}$ and W $4f_{7/2}$ are presented.

Compound	XPS Peak Positions (Binding Energy, eV)									
	Ga 2p _{1/2}	Ga 2p _{3/2}	O 1s	Fe 2p _{1/2}	Fe 2p _{3/2}	Ti 2p _{1/2}	Ti 2p _{3/2}	W 4f _{5/2}	W 4f _{7/2}	
Intrinsic Ga ₂ O ₃	1144.47	1117.58	530.61	_	_	_	_	_	_	
Fe-doped Ga ₂ O ₃	1144.39	1117.56	530.56	724.84	711.18	-	_	_	_	
Ti-doped Ga ₂ O ₃	1143.67	1117.28	530.64	-	-	464.51	458.78	-	-	
W-doped Ga ₂ O ₃	1144.62	1117.75	530.67	-	_	-	_	37.71	35.53	

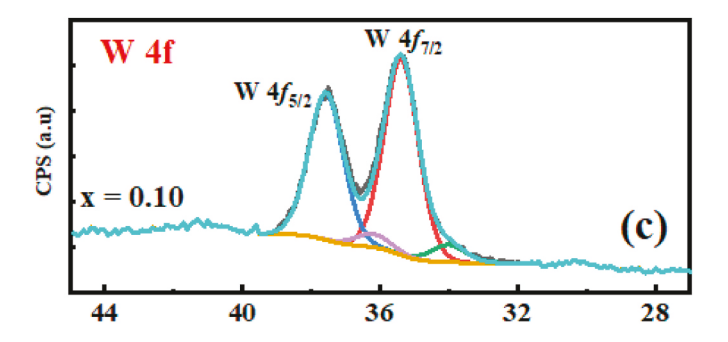
Table 3
Comparison of FWHM of Ga 2p, O 1s, and TM element core-level spectra.

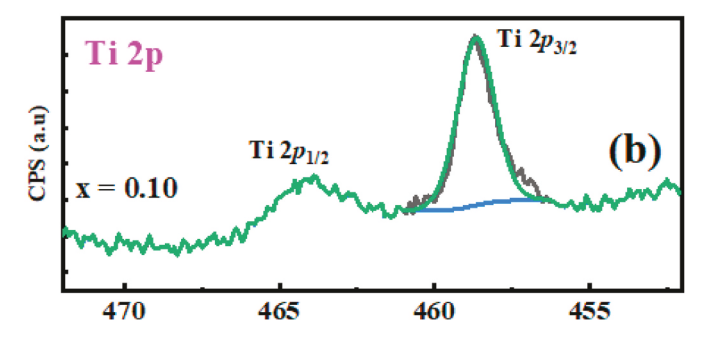
Compounds	FWHM (eV)					
	Ga 2p _{3/2}	O 1s	Fe 2p _{3/2} /Ti 2p _{3/2} /W 4f _{7/2}			
Ga ₂ O ₃	1.40	1.51	_			
GFO	1.40	1.49	1.6			
GWO	1.40	1.51	1.7			
GTO	1.40	1.50	1.5			

provide a signature identification of specific iron oxide phases and chemical states [64,69]. For the Fe³⁺ chemical state in Fe₂O₃, the Fe 2p_{3/2} core-level XPS peak exhibits a shake-up satellite at 719–720 eV [63,66–69], whereas it is at 715–716 eV for the Fe²⁺ chemical state in FeO [66,68]. However, the Fe ions in Fe₃O₄ (magnetite) comprise 1/3 Fe²⁺ ions and 2/3 Fe³⁺ ions [69], and show no satellite structure [66,69]. Thus, for Fe doping up to x = 0.1 in the Ga₂O₃ samples, it is evident that Fe exhibits mixed valence states (Fe³⁺ and Fe²⁺). Nevertheless, the major intensity component Fe 2p_{3/2} peak at ca. 711 eV and the shake-up satellite peak at ca. 720 eV indicate that the Fe ions doped in Ga₂O₃ are predominantly in the Fe³⁺ chemical state, with only a small proportion present as Fe²⁺.

Further changes in the electronic structure of Fe-doped Ga_2O_3 with increasing Fe content (x) are evident, as reflected in the chemical changes in the Fe 2p core-level spectra shown in Fig. 6 (a). Contrary to the mixed chemical states of Fe observed for x=0.1, only the highest chemical state (Fe³⁺) is evident at x=0.2. Considerable iron content may drive the formation of a stoichiometric and charge-balanced Fedoped Ga_2O_3 compound. With increasing iron content in the Ga_2 - xFe_xO_3 compounds, the intensity of the Fe peak increases. In addition, a shake-up satellite peak is seen at around 720 eV, in accordance with literature data [61,69], which is a characteristic feature of Fe³⁺ in α -Fe₂O₃. Thus, XPS studies indicate the formation of single-phase Ga_2 - xFe_xO_3 compounds, in which Fe substitutes Ga and charge balance drives the overall compound formation.

High-resolution XPS patterns [Fig. 5 (b) and 6 (b)] of Ti 2p reveal the chemistry of the Ti in Ga_2O_3 . Fig. 5 (b) shows the Ti 2p core-level XPS pattern of the Ti-mixed Ga_2O_3 with x=0.1, and Fig. 6 (b) shows that of the compound with x=0.2. For simplicity and clarification, we consider first the Ti 2p core-level XPS pattern for the Ti-GO compound with x=0.1 [Fig. 5 (b)]. Similarly to Ga 2p and Fe 2p XPS, the Ti 2p pattern also exhibits the characteristic doublet of Ti $2p_{3/2}$ and Ti $2p_{1/2}$. The doublet in the Ti 2p pattern arises from spin-orbit splitting [62–68]. The BES





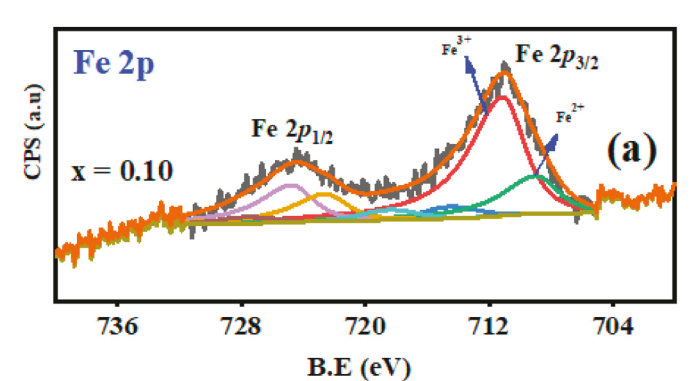


Fig. 5. Fe 2p, Ti 2p, and W 4f core-level XPS patterns of TM-GO (TM = Fe, Ti, W; x=0.1) compounds.

(Table 1) of Ti $2p_{3/2}$ and Ti $2p_{1/2}$ are around 458.7 and 464.4 eV,

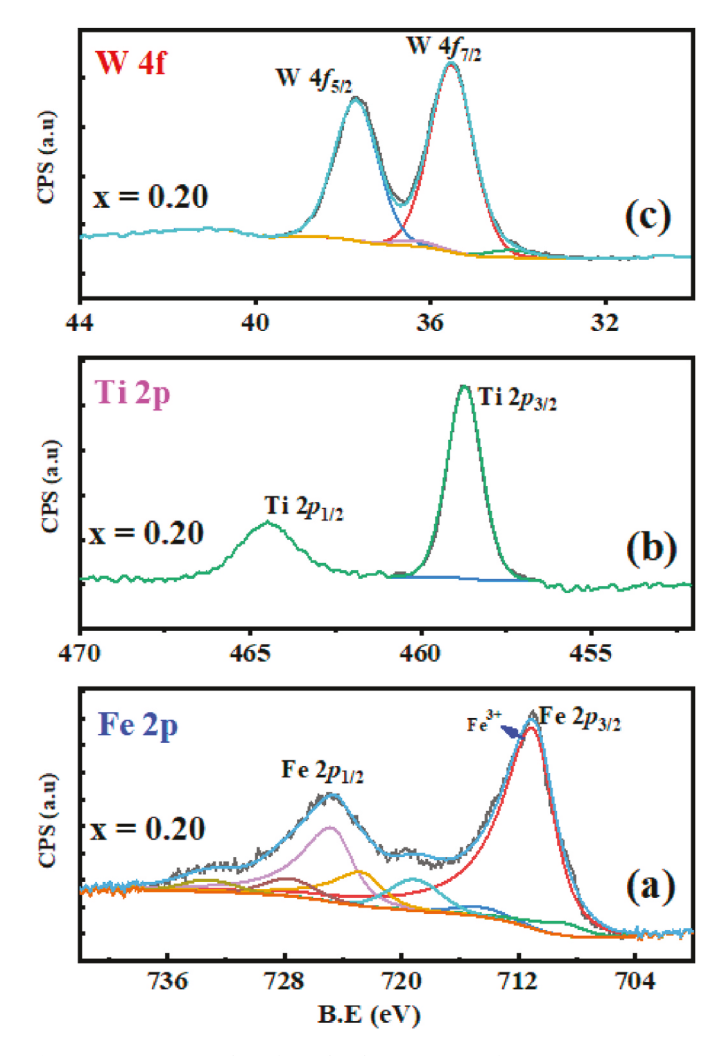


Fig. 6. Fe 2p, Ti 2p, and W 4f core-level XPS patterns of TM-GO (M = Fe, Ti, W; x = 0.2) compounds with a higher dopant content.

respectively. Titanium can adopt multiple valence states, namely Ti⁴⁺, Ti^{3+} , Ti^{2+} , and Ti^{0} [46,47,70,71,72,73,75]. The reduced Ti states may be the result of defects. In addition, it is possible for Ti⁴⁺, Ti³⁺, Ti²⁺, and Ti⁰ states to co-exist [46,70,72,73]. Therefore, peak-fitting and deconvolution of Ti 2p XPS peaks requires the utmost care. The three most important characteristic features noted for the Ti 2p XPS peak of all of the Ti-GO compounds are the following. (1) The deconvolution (peak-fitting) of the Ti 2p_{3/2} core-level XPS pattern results in a single symmetric peak. (2) The Ti $2p_{3/2}$ peak is centered at a BE of ca. 458.7 eV. (3) The spin-orbit splitting energy parameter, that is, the energy separation of the Ti $2p_{3/2}$ and Ti $2p_{1/2}$ peaks, $\Delta E(\text{Ti }2p)$, is about 5.75 eV. These characteristic features indicate that Ti exists in its tetravalent state (Ti⁴⁺) in all of the Ti-GO compounds. Furthermore, the formation of stoichiometric TiO2 with a low level of defects is generally responsible for the symmetric nature of Ti 2p peaks [75,76]. Thus, in the present case, the deconvolution (peak-fitting) of the Ti 2p3/2 core-level XPS pattern results in a single peak, which confirms the absence of other valence states of Ti. Usually, if Ti occupies Ga sites, that is, Ti³⁺ for Ga³⁺ in the gallium oxide structure, there should be corresponding components in both the O 1s and Ti 2p peaks. However, this is not seen here, and none of the components can be confidently assigned to Ti-O bonds related to Ti₂O₃. Thus, XPS core-level analysis of the Ti-GO compounds clearly rules out the possibility of single-phase compounds. A closer look at the component peak data in the XPS pattern of Ti 2p gives an insight into the formation kinetics of the Ga_2O_3 - TiO_2 composite. The $Ti\ 2p_{3/2}$ peaks at BEs of 458.6 and 457.13 eV correspond to the Ti⁴⁺ and Ti³⁺

valence states, respectively [46,47,70,72,73,74]. Ti⁴⁺ does not have an unpaired d electron that can be made available for multiplet splitting, whereas Ti³⁺ has unpaired d electrons that may give rise to unresolved multiplet structures [77]. The XPS data for the Ti-GO samples show the presence of TiO2, which corroborates the formation of Ga2O3-TiO2 composite [40]. For the scope of the present work, we have excluded the low oxidation states of Ti (Ti²⁺ and Ti⁰), for which no components of appreciable intensity are seen. The benefits of, and insights from, fitting of the Ti 2p_{3/2} peaks, along with the simplicity, far outweigh the fitting of the Ti $2p_{1/2}$ peaks. Indeed, Ti $2p_{1/2}$ peaks cannot be fitted with high confidence [73]. It can clearly be seen that there is no appreciable change when the Ti content is raised to x = 0.20 [Fig. 6 (b)] and it can be reliably concluded that a Ga_2O_3 -TiO₂ composite is formed at all xvalues. These claims are further substantiated by data reported for Ti-Ga₂O₃ thin films deposited by a physical vapor deposition method [40]. This study showed the effect of Ti doping on the local microstructure and the chemical properties [40]. Besides XPS data, TEM images also revealed how increasing sputtering power at the Ti target assisted the formation of Ga₂O₃-TiO₂ films in the presence of Ti⁴⁺ ions. XRD studies also revealed the formation of a single-phase nanocrystalline thin film for both undoped β-Ga₂O₃ and low-level Ti-doped thin films [40]. XRD also showed a remarkable trend upon Ti doping of Ga₂O₃, whereby peak broadening and merging occurred, which was ascribed to Ga₂O₃-TiO₂ formation [40,78].

Detailed core-level XPS patterns of W 4f for the W-GO compounds with x = 0.1 and x = 0.2 are shown in Fig. 5 (c) and 6 (c), respectively. Again, for the sake of clarity and simplicity, we consider first the data for x = 0.1 and subsequently consider those for x = 0.2 to explain the effect of increasing W content on the electronic structure. The W 4f core-level XPS pattern of the W-GO compound with x = 0.1 [Fig. 5 (c)] shows a well-resolved doublet corresponding to W $4f_{5/2}$ at BE $\approx 37.5~\text{eV}$ and W $4f_{7/2}$ at BE ≈ 35.4 eV. The spin-orbit splitting energy separation $\Delta E(W)$ 4f) is ca. 2.1 eV. The W $4f_{7/2}$ peak at 35.4 eV seen for W-GO compounds is in good agreement with the literature (35.4 eV) and characterizes the existence of W ions in the W⁶⁺ state [48, 49, 81, 82]. Furthermore, the spin-orbit splitting of ca. 2.1 eV with an almost 4:3 ratio between the W $4f_{7/2}$ and W $4f_{5/2}$ levels also validates the existence of W in its highest chemical oxidation state (W⁶⁺) [49,78,79] in the W-GO compounds. As widely documented in the literature, W can exhibit multiple valence states, namely W⁶⁺, W⁵⁺, W⁴⁺, and W⁰ [49], [81–83]. Additionally, due to variation in thermodynamic conditions and/or processing physical/chemical parameters, W⁶⁺, W⁵⁺, W⁴⁺, and W⁰ can co-exist, which can further complicate interpretation. Furthermore, recent theoretical work and calculations by Peelaers et al. [31] point to multiple oxidation states for W as a dopant in Ga₂O₃, although the doping levels considered were very different. Therefore, we paid utmost attention to evaluating the chemical state of W in these W-GO compounds, to ascertain whether it was wholly in the W⁶⁺ state or existed as a mixture of lower valence states. BEs of the W 4f_{7/2} peak for reduced states reported in the literature are 34.5, 32.7, and 31.0 eV for W⁵⁺, W⁴⁺, and W⁰, respectively [49], [81-83]. Furthermore, the presence of reduced states or the co-existence of mixed valence states of W will result in broadening of the W 4f peak. It is abundantly clear that components related to reduced W states are absent in the deconvolution of the W 4f doublet, and that no appreciable peak intensity in the lower BE region corresponds to metallic W. This leads to a logical exclusion of reduced W states, viz. W^{5+} , W^{4+} , and W^{0} . It is worth noting the subtle peak broadening of the W 4f doublet at lower W doping levels [30], which can be attributed to some W ions adopting a lower valence state. The deconvoluted W 4f core-level XPS pattern points to a mixture of W4+ and W6+ at low W-doping levels, consistent with the peak-fitting. This phenomenon was observed predominantly for x = 0.05 [30]. As the W content is increased, it is clear from the core-level W 4f spectra that lower-valence-state W ions are no longer seen. However, the W-GO sample with x = 0.30 exhibits a shift of 0.30 eV in the W 4f peak, which can be traced back to the different stages of sample preparation. The W

4f XPS data are in full agreement with findings from XRD reported previously [3]. The W incorporation in $\beta\text{-}Ga_2O_3$ is essentially substitution by W ions in Ga ion sites. Charge imbalance leads to some W ions being present in a lower valence state, which is not detectable by XRD. On the other hand, it has been hypothesized that mass transportation is assisted by the formation of W ions of different chemical valence. Therefore, a limited amount of W enters the Ga_2O_3 phase, while the bulk of the W oxide forms a secondary phase, as evidenced at a higher content of WO_3 . This phenomenon is also evidenced by the XPS data.

Fig. 6 (c) shows high-resolution XPS data for W 4f in the W-GO compound with a higher dopant concentration (x=0.2). The W 4f peak XPS data of the TM-GO compounds are presented in Table 2. The features of the W 4f peaks at x=0.2 are essentially the same as those at x=0.1. A well-resolved doublet due to spin-orbit splitting with a separation of 2.1 eV, with the W 4f_{7/2} peak at BE ≈ 35.4 eV, verifies that the W ions are in their highest oxidation state of W⁶⁺ in these compounds.

Finally, we attempted to produce TM-GO compounds with higher values of x to assess the effect of composition on electronic structure and chemical bonding environment. However, such studies were limited to TM = Fe and W because higher loadings of Ti were found to result in the separation of a secondary phase of TiO₂. Thus, only TM-GO (TM = Fe, W) compounds were synthesized with higher x values up to 0.3, and submitted to XPS measurements. The XPS survey spectra of TM-GO (x > 0.2; M = Fe, W; not shown) are very similar to those obtained for the $Ga_{2-x}M_xO_3$ (M = Fe, W) compounds with lower x values (Fig. 1a and b). Similar to the XPS data presented in Fig. 1a and b, characteristic XPS peaks due to Ga and O are seen for all of the samples, along with the respective dopant (Fe and W) peaks. The electronic structures and chemical compositions for x = 0.3 were further probed through detailed high-resolution XPS scans of the Ga, O, Fe, and W core levels, as presented and discussed below.

The Ga 2p core-level XPS patterns are shown in Fig. 7. As for the

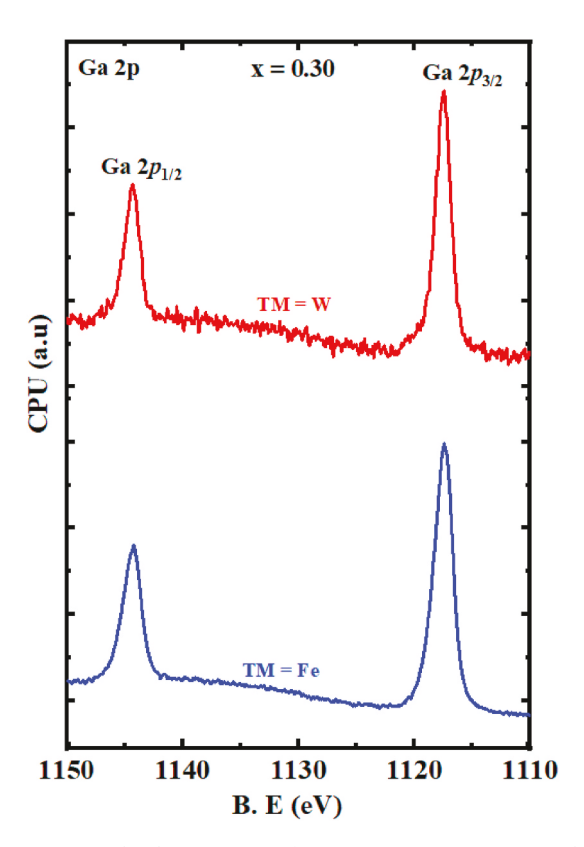


Fig. 7. Ga 2p core-level XPS patterns of TM-GO (TM = Fe, W) compounds with x=0.3. Similar to the XPS data for x=0.0–0.2, the Ga 2p data reveal that no significant changes occur even with a higher content of transition metal doping in $\rm Ga_2O_3$.

compounds with x=0.1 and x=0.2, the Ga 2p region at x=0.3 shows the Ga 2p doublet, i.e., the Ga 2p_{3/2} and Ga 2p_{1/2} peaks, at BEs of 1117.5 and 1144.2 eV, respectively. Thus, no changes in BE location and/or peak shape were observed for the Ga 2p region as a function of Fe or W mixing in TM-GO compounds up to x=0.3. Again, the core-level XPS data for Ga 2p confirm that all Ga ions exist in the highest oxidation state (Ga³⁺) in these compounds. Considering all of the collected data, it can be concluded that the chemical state of Ga is unaffected by different dopants at loadings up to x=0.3.

High-resolution XPS patterns of O 1s in the TM-GO (TM = Fe, W; x = 0.3) compounds are shown in Fig. 8. As for the other compositions, the O 1s peak is asymmetric and is dominated by an intense peak at BE \approx 530.7 eV, corresponding to Ga–O bonds [53,54,58–60], as expected for stoichiometric Ga₂O₃. Shoulder peaks seen at BEs of 532.2 and 533.4 eV can be attributed to surface oxygen bound to carbon in the form of either carbonyl (oxygen bonded to carbon, C–O) or hydroxyl (oxygen bonded to hydrogen, O–H) groups [56,57]. Again, these functional groups may be adsorbed on the sample surface as impurities during sample transfer from the fabrication chamber and/or furnace atmosphere to the XPS load lock [53,56,57].

High-resolution core-level XPS scans of Fe 2p and W 4f are presented in Fig. 9. The data correspond to the characteristic bonding and chemical state of the respective dopant cations in Ga_2O_3 [40,53] The Fe 2p region [Fig. 9 (a)] shows the typical Fe $2p_{3/2}$ and Fe $2p_{1/2}$ doublet peaks, a characteristic feature of spin-orbit splitting. Inspection of the BE positions of the Fe $2p_{3/2}$ and Fe $2p_{1/2}$ peaks reveals the presence of Fe³⁺. We hypothesize that charge-balanced Fe– Ga_2O_3 compounds arise from the presence of Fe³⁺ at higher concentrations as opposed to a mixed chemical state at lower Fe concentration. The W 4f XPS data [Fig. 9 (b)] imply similar dopant chemistry in Ga_2O_3 as the core-level W 4f pattern is devoid of any component pertaining to a lower valence state of W ions at x=0.3. The XPS data for x=0.3 reveal a positive shift of 0.30 eV in the W 4f peak, which can be attributed to the numerous steps involved in

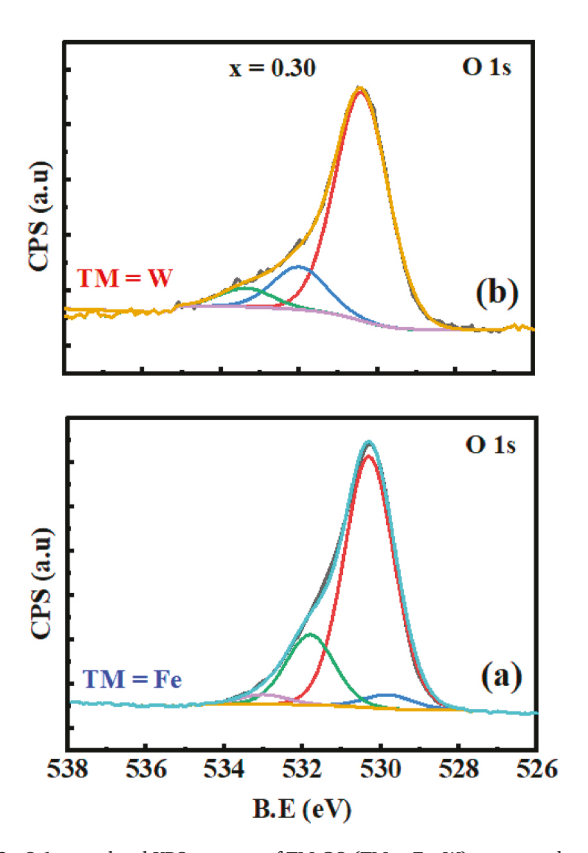


Fig. 8. O 1s core-level XPS patterns of TM-GO (TM = Fe, W) compounds with a higher dopant content, x = 0.3.

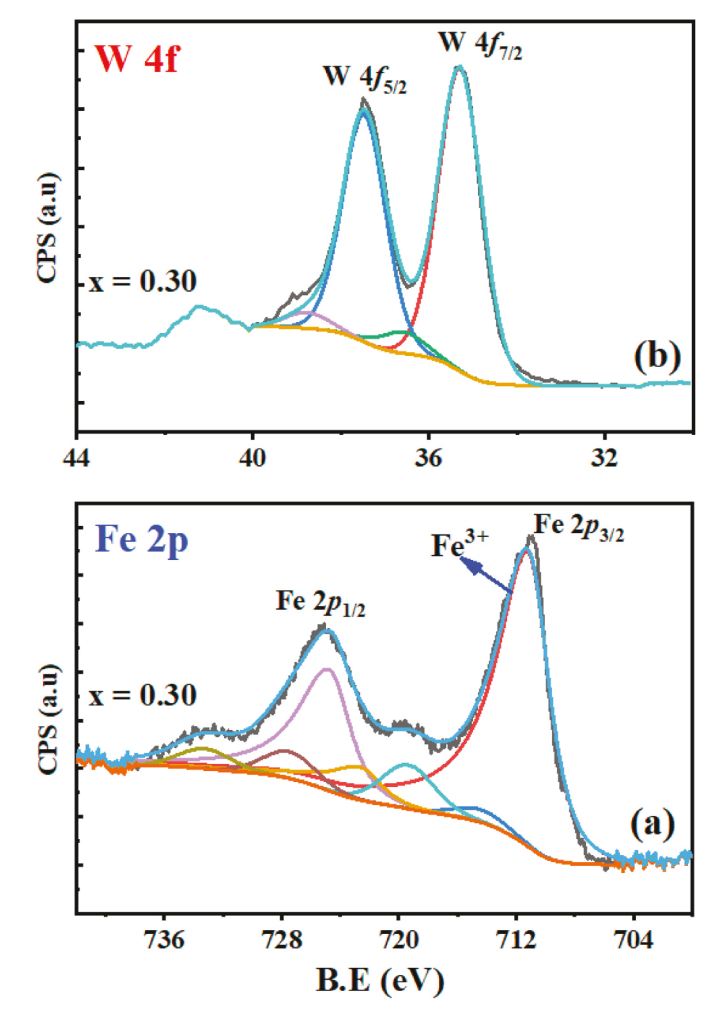


Fig. 9. Fe 2p and W 4f core-level XPS patterns of TM-GO (TM = Fe, W) for x = 0.3.

sample fabrication. The XPS data for W are in full agreement with those reported previously [30].

Finally, to summarize the findings and provide a road-map for considering transition-metal-doped $\beta\text{-}\text{Ga}_2\text{O}_3$ for practical applications, a schematic diagram explaining the electronic structure modification of the material by means of various transition metal ions is presented in Fig. 10. As shown in Fig. 10, in the monoclinic unit cell of Ga₂O₃, Ga atoms (green) are either tetrahedrally or octahedrally coordinated by oxygen atoms (red). The oxygen atoms can occupy three different lattice sites in the distorted cubic close-packed arrangement around the Ga sites [20,41]. Transition metal ions, specifically Fe, Ti, and W ions as considered in this work, are capable of manipulating the structure and electronic properties. Of these TM ions, Fe ions can enter the Ga sites to form single-phase and charge-balanced Ga_{2-x}Fe_xO₃ compounds. However, low-level doping of Fe in Ga₂O₃ induces defects, which can be attributed to the formation of Fe mixed valence states (Fe $^{3+}$ and Fe $^{2+}$). As the Fe content is increased, all of the Fe exists as Fe³⁺. For Ti, Ga₂O₃-TiO₂ composite formation occurs over the entire range of compositions. No reduced states of Ti are found. For W, its solubility in Ga₂O₃ is very limited. W⁵⁺ and W⁶⁺ states may be formed, some of which can substitute Ga, resulting in the formation of Ga₂O₃-WO₃ composite on further increasing the W content.

4. Conclusions

Transition metal (TM)-mixed gallium oxide (Ga₂O₃) (TM = Fe, Ti, W;

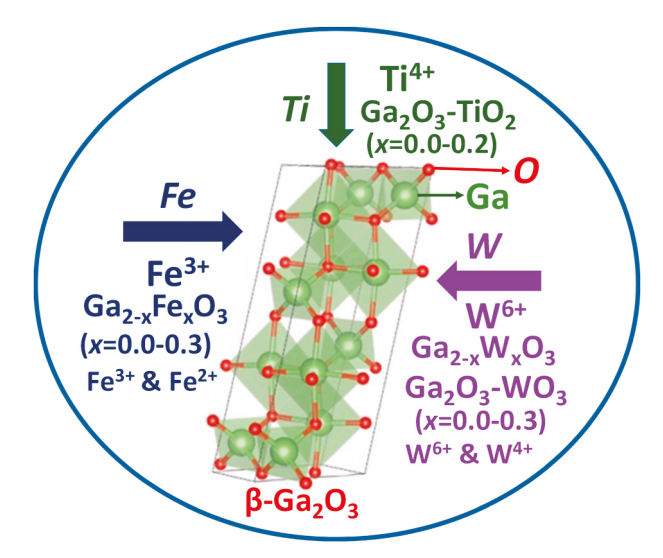


Fig. 10. Schematic diagram summarizing the effects of various transition metal ions on the electronic properties of ${\rm Ga_2O_3}$.

 $0.00 \le x \le 0.30$) polycrystalline compounds have been synthesized by a conventional high-temperature solid-state reaction method. The effects of Fe-, Ti-, and W-doping on the electronic properties and chemical bonding of the resulting TM-GO compounds have been studied in detail. X-ray photoelectron spectroscopy (XPS) measurements have revealed that the chemical states of Fe, Ti, and W ions vary in the TM-GO compounds as a function of TM concentration. The electronic structures and chemical states of the respective ions are very different when Fe, Ti, or W is mixed in Ga_2O_3 . Mixed valence states of the respective TM ions (Fe²⁺/ Fe³⁺, W⁴⁺/W⁶⁺) have been evidenced in the single-phase TM-GO compounds upon initial or low-level Fe- or W-doping. Conversely, Timixed Ga₂O₃ compounds only feature dopant Ti ions in their highest valence state (Ti⁴⁺) over the entire range of doping contents. Although both Fe and W adopt mixed valence states at lower doping levels, the chemical state evolution is different for Fe and W ions at increased dopant levels. High levels of Fe doping lead to exclusively Fe³⁺ states being present, and all Fe-mixed Ga₂O₃ compounds exist as a single phase. W ions also adopt the highest valence state (W^{6+}) at higher x values, but Ga₂O₃-WO₃ composite formation occurs at higher W content. Ga ions exist in their highest valence state (Ga³⁺) in all of the TM-GO compounds and for all x values.

Author contributions and statement

CVR conceived and supervised the research. SR, VZ, AKB, NM synthesized samples. SR and VS collected the XPS data on all of the samples. CVR coordinated the project and scientific contributions from all the authors. CVR put together all the data analyses etc into the manuscript. All authors were involved in data analyses, designed figures, and wrote the manuscript. CVR coordinated to collect the comments and feedback from all co-authors. Finally, all the authors approved the submission.

Declaration of competing interest

The authors declare that they have no known competing financial interests or personal relationships that could have appeared to influence the work reported in this paper.

Acknowledgments

The authors gratefully acknowledge support from the National Science Foundation (NSF) through NSF-PREM grant #DMR-1827745. Some of this work and material is also based upon work supported by the

Air Force Office of Scientific Research under award number FA9550-18-1-0387. However, any opinions, finding, and conclusions or recommendations expressed in this material are those of the author(s) and do not necessarily reflect the views of the United States Air Force. The authors sincerely thank Dr. M. Bandi for technical assistance in sample preparation and structural analyses. A portion of the research (XPS measurements) was performed using Environmental Molecular Sciences Laboratory (EMSL), a national scientific user facility sponsored by the Department of Energy's Office of Biological and Environmental Research and located at Pacific Northwest National Laboratory.

Appendix A. Supplementary data

Supplementary data to this article can be found online at https://doi.org/10.1016/j.jpcs.2021.110174.

References

- [1] S.J. Pearton, J. Yang, P.H. Cary, F. Ren, J. Kim, J.M. Tadjer, M.A. Mastro, A review of Ga₂O₃ materials, processing, and devices, Appl. Phys. Rev. 5 (2018), 011301-011356.
- [2] M. Higashiwaki, G.H. Jessen, Guest editorial: the dawn of gallium oxide microelectronics, Appl. Phys. Lett. 112 (2018), 060401.
- [3] V. Zade, B. Mallesham, S. Shantha-Kumar, A. Bronson, C.V. Ramana, Interplay between solubility limit, structure, and optical properties of tungsten-doped Ga₂O₃ compounds synthesized by a two-step calcination process, Inorg. Chem. 58 (2019) 3707–3716
- [4] Y. Usui, D. Nakauchi, N. Kawano, G. Okada, N. Kawaguchi, T. Yanagida, Scintillation and optical properties of Sn-doped Ga₂O₃ single crystals, J. Phys. Chem. Solid. 117 (2019) 36–47.
- [5] G. Sinha, A. Patra, Generation of green, red and white light from rare-earth doped Ga₂O₃ nanoparticles, Chem. Phys. Lett. 473 (2009) 151–154.
- [6] X.H. Wang, F.B. Zhang, K. Saito, T. Tanaka, M. Nishio, Q.X. Guo, Electrical properties and emission mechanisms of Zn-doped β-Ga₂O₃ films, J. Phys. Chem. Solid. 75 (2014) 1201–1204.
- [7] S. Ghose, S. Rahman, L. Hong, J.S. Rojas-Ramirez, H. Jin, K. Park, R. Klie, R. Droopad, Growth and characterization of β-Ga₂O₃ thin films by molecular beam epitaxy for deep-UV photodetectors, J. Appl. Phys. 122 (2017), 095302.
- [8] S.B. Patil, I.Y. Kim, J.L. Gunjakar, S.M. Oh, T. Eom, H. Kim, S.J. Hwang, Phase tuning of nanostructured gallium oxide via hybridization with reduced graphene oxide for superior anode performance in Li-ion battery: an experimental and theoretical study, ACS Appl. Mater. Interfaces 7 (2015) 18679–18688.
- [9] M. Ogita, K. Higo, Y. Nakanishi, Y. Hatanaka, Ga₂O₃ thin film for oxygen sensor at high temperature, Appl. Surf. Sci. 175 (2001) 721–725.
- [10] S.-E. Choi, Y.-T. Oh, H.-K. Ham, T.-W. Kim, B.-H. Choi, D.-C. Shin, Work function control of functionally graded ZnO + Ga₂O₃ thin film for OLED applications, Curr. Appl. Phys. 11 (2011) S255–S257.
- [11] C.V. Ramana, Properties of sputter-deposited gallium oxide, in: Gallium Oxide, Elsevier, 2019, pp. 47–66.
- [12] H. He, R. Orlando, M.A. Blanco, R. Pandey, E. Amzallag, I. Baraille, M. Rérat, First-principles study of the structural, electronic, and optical properties of Ga₂O₃ in its monoclinic and hexagonal phases, Phys. Rev. B 74 (19) (2006), 195123.
- [13] S.S. Kumar, E.J. Rubio, M. Noor-A-Alam, G. Martinez, S. Manandhar, V. Shutthanandan, S. Thevuthasan, C.V. Ramana, Structure, morphology, and optical properties of amorphous and nanocrystalline gallium oxide thin films, J. Phys. Chem. C 117 (2013) 4194–4200.
- [14] W. Zhang, B.S. Naidu, J.Z. Ou, A.P. O'Mullane, A.F. Chrimes, B.J. Carey, Y. Wang, S.Y. Tang, V. Sivan, A. Mitchell, S.K. Bhargava, K. Kalantar-Zadeh, Liquid metal/metal oxide frameworks with incorporated Ga₂O₃ for photocatalysis, ACS Appl. Mater. Interfaces 7 (2015) 1943–1948.
- [15] J. Liu, G. Zhang, Mesoporous mixed-phase Ga₂O₃: green synthesis and enhanced photocatalytic activity, Bull. Mater. Res. 68 (2015) 254–259.
- [16] H. Sun, K.-H. Li, C.G. Torres Castanedo, S. Okur, G.S. Tompa, T. Salagaj, S. Lopatin, A. Genovese, X. Li, HCl flow-induced phase change of α-, β-, and ε-Ga₂O₃ films grown by MOCVD, cryst, Growth & Design 184 (2018) 2370–2376.
- [17] Y. Chen, X. Xia, H. Liang, Q. Abbas, Y. Liu, G. Du, Growth pressure controlled nucleation epitaxy of pure phase ε- and β-Ga₂O₃ films on Al₂O₃ via metal–organic chemical vapor deposition, Cryst. Growth Des. 18 (2018) 1147–1154.
- [18] S. Yoshioka, H. Hayashi, A. Kuwabara, F. Oba, K. Matsunaga, I. Tanaka, Structures and energetics of Ga₂O₃ polymorphs, J. Phys. Condens. Matter 19 (2007), 346211.
- [19] H. He, R. Orlando, M.A. Blanco, R. Pandey, E. Amzallag, I. Baraille, M. Rérat, First-principles study of the structural, electronic, and optical properties of Ga₂O₃ in its monoclinic and hexagonal phases, Phys. Rev. B 74 (2006), 195123.
- [20] J. Åhman, G. Svensson, J. Albertsson, A reinvestigation of β-gallium oxide, Acta Crystallogr. C 52 (1996) 1336–1338.
- [21] M. Bartic, C.I. Baban, H. Suzuki, M. Ogita, M. Isai, β-Gallium oxide as oxygen gas sensors at a high temperature, J. Am. Ceram. Soc. 90 (9) (2009) 2879–2884.
- [22] H.J. Lin, J.P. Baltrus, H. Gao, Y. Ding, C.Y. Nam, P. Ohodnicki, P.X. Gao, Perovskite nanoparticle-sensitized Ga₂O₃ nanorod arrays for CO detection at high temperature, ACS Appl. Mater. Interfaces 8 (2016) 8880–8887.

- [23] H. Peelaers, C.G. Van de Walle, Brillouin zone and band structure of β-Ga₂O₃, Phys. Status Solidi 252 (2015) 828–832.
- [24] Y. Yao, R.F. Davis, L.M. Porter, Investigation of different metals as ohmic contacts to β-Ga₂O₃: comparison and analysis of electrical behavior, morphology, and other physical properties, J. Electron. Mater. 46 (2017) 2053–2060.
- [25] G. Yang, S. Jang, F. Ren, S.J. Pearton, J. Kim, Influence of high-energy proton irradiation on β-Ga₂O₃ nanobelt field-effect transistors, ACS Appl. Mater. Interfaces 9 (2017) 40471–40476.
- [26] M. Bandi, V. Zade, S. Roy, A.N. Nair, S. Seacat, S. Sreenivasan, V. Shutthanandan, C.G. Van de Walle, H. Peelaers, C.V. Ramana, Effect of Ti induced chemical inhomogeneity on crystal structure, electronic structure and optical properties of wide band gap Ga₂O₃, Cryst . Growth & Des. 20 (2020) 1422–1433.
- [27] S. Hong, C.K. Rhee, Y. Son, Photoluminescence, electro- and thermal catalytic properties of bare and Eu(III)-doped GaOOH, α- and β-Ga₂O₃ nanorods, J. Alloys Compd. 774 (2017) 11–17.
- [28] Z. Gao, X. Lu, Y. Chu, S. Guo, L. Liu, Y. Liu, S. Sun, J. Ren, J. Yang, The distribution of rare earth ions in a γ-Ga₂O₃ nanocrystal-silicate glass composite and its influence on the photoluminescence properties, RSC Adv. 6 (2018) 2944–2950.
- [29] S. Roy, B. Mallesham, V.B. Zade, A. Martinez, V. Shutthanandan, S. Thevuthasan, C.V. Ramana, Correlation between structure, chemistry, and dielectric properties of iron-doped gallium oxide (Ga_{2-x}Fe_xO₃), J. Phys. Chem. C 122 (2018) 27597–27607.
- [30] V. Zade, B. Mallesham, S. Roy, V. Shutthanandan, C.V. Ramana, Electronic structure of tungsten-doped β -Ga₂O₃ compounds, ECS J. Solid State Sci. Technol. 8 (2019) Q3111–Q3115.
- [31] H. Peelaers, C.G. Van De Walle, Doping of Ga_2O_3 with transition metals, Phys. Rev. B 94 (2016), 195203.
- [32] C. Tang, J. Sun, N. Lin, Z. Jia, W. Mu, X. Tao, X. Zhao, Electronic structure and optical property of metal-doped Ga₂O₃: a first principles study, RSC Adv. 6 (2016) 78322–78334.
- [33] E.G. Víllora, K. Shimamura, Y. Yoshikawa, T. Ujiie, K. Aoki, Electrical conductivity and carrier concentration control in β -Ga₂O₃ by Si doping, Appl. Phys. Lett. 92 (2008), 202118.
- [34] X. Wang, S. Shen, S. Jin, J. Yang, M. Li, X. Wang, H. Han, C. Li, Effects of Zn²⁺ and Pb²⁺ dopants on the activity of Ga₂O₃-based photocatalysts for water splitting, Phys. Chem. Chem. Phys. 15 (2013) 19380–19386.
- [35] Y. Zhang, J. Yan, Q. Li, C. Qu, L. Zhang, W. Xie, Optical and structural properties of Cu-doped β-Ga₂O₃ films, Mater. Sci. Eng. B 176 (2011) 846–849.
- [36] H. Zhang, J. Deng, P. Duan, R. Li, Z. Pan, Z. Bai, L. Kong, J. Wang, Effect of Au nanoparticles on the optical and electrical properties of Nb-doped β-Ga₂O₃ film, Vacuum 155 (2018) 465–469.
- [37] A.A. Dakhel, Structural, optical, and opto-dielectric properties of W-doped Ga_2O_3 thin films, J. Mater. Sci. 47 (2012) 3034–3039.
- [38] E.J. Rubio, T.E. Mates, S. Manandhar, M. Nandasiri, V. Shutthanandan, C. V. Ramana, Tungsten incorporation into gallium oxide: crystal structure, surface and interface chemistry, thermal stability, and interdiffusion, J. Phys. Chem. C 120 (2016) 26720–26735.
- [39] E.J. Rubio, C.V. Ramana, Tungsten-incorporation induced red-shift in the bandgap of gallium oxide thin films, Appl. Phys. Lett. 102 (2013), 191913.
 [40] S. Manandhar, A.K. Battu, S. Tan, R. Panat, V. Shutthanandan, C.V. Ramana, Effect
- [40] S. Manandhar, A.K. Battu, S. Tan, R. Panat, V. Shutthanandan, C.V. Ramana, Effect of Ti doping on the crystallography, phase, surface/interface structure and optical band gap of Ga₂O₃ thin films, J. Mater. Sci. 54 (2019) 11526–11537.
- [41] S. Geller, Crystal structure of β-Ga₂O₃, J. Chem. Phys. 33 (1960) 676–684.
- [42] Y. Tomm, P. Reiche, D. Klimm, T. Fukuda, Czochralski grown Ga₂O₃ crystals, J. Cryst. Growth 220 (2000) 510–514.
- [43] B. Mallesham, S. Roy, S. Bose, A.N. Nair, S. Sreenivasan, V. Shutthanandan, C. V. Ramana, Crystal chemistry, band-gap red shift, and electrocatalytic activity of iron-doped gallium oxide ceramics, ACS Omega 5 (2019) 104–112.
- [44] G. Carbajal-Franco, M. Eastman, C.V. Ramana, Structure and optical properties of iron oxide films prepared by a modified wet-chemical method, Ceram. Int. 39 (2013) 4581–4587.
- [45] C.R. Cornell, U. Schwertmann, The Iron Oxides: Structure, Properties, Reactions, Occurrences and Uses, Wiley-VCH, Weinheim, 2000.
- [46] M.J. Jackman, A.G. Thomas, C. Muryn, Photoelectron spectroscopy study of stoichiometric and reduced anatase TiO₂(101) surfaces: the effect of subsurface defects on water adsorption at near-ambient pressures, J. Phys. Chem. C 119 (2015) 13682–13690.
- [47] E. Wang, W. Yang, Y. Cao, Unique surface chemical species on indium-doped TiO₂ and their effect on the visible light photocatalytic activity, J. Phys. Chem. C 113 (2009) 20912–20917.
- [48] R.S. Vemuri, M.H. Engelhard, C.V. Ramana, Correlation between surface chemistry, density, and band gap in nanocrystalline WO₃ thin films, ACS Appl. Mater. Interfaces 4 (2012) 1371–1377.
- [49] Z. Li, Z. Zhang, Y.K. Kim, R.S. Smith, F. Netzer, B.D. Kay, R. Rousseau, Z. Dohnalek, Growth of ordered ultrathin tungsten oxide films on Pt(111), J. Phys. Chem. C 115 (2011) 5773–5783.
- [50] C.V. Ramana, A.K. Battu, P. Dubey, G.A. Lopez, Phase-control-enabled enhancement in hydrophilicity and mechanical toughness in nanocrystalline tungsten oxide films for energy-related applications, ACS Appl. Nano Mater. 3 (4) (2020) 3264–3274.
- [51] J.F. Moulder, J. Chastain, Handbook of X-Ray Photoelectron Spectroscopy: A Reference Book of Standard Spectra for Identification and Interpretation of XPS Data, Physical Electronics Division, Perkin-Elmer Corporation, 1995.
- [52] S.E. Shirsath, C. Cazorla, T. Lu, L. Zhang, Y.Y. Tay, X. Lou, Y. Liu, S. Li, D. Wang, Interface-charge induced giant electrocaloric effect in lead-free ferroelectric thinfilm bilayers, Nano Lett. 20 (2) (2019) 1262–1271.

- [53] C.V. Ramana, E.J. Rubio, C.D. Barraza, A. Miranda Gallardo, S. McPeak, S. Kotru, J. T. Grant, Chemical bonding, optical constants, and electrical resistivity of sputter-deposited gallium oxide thin films, J. Appl. Phys. 115 (2014), 043508.
- [54] W. Priyantha, G. Radhakrishnan, R. Droopad, M. Passlack, In situ XPS and RHEED study of gallium oxide on GaAs deposition by molecular beam epitaxy, J. Cryst. Growth 323 (2011) 103–106.
- [55] V.V. Atuchin, L.D. Pokrovsky, O. Yu Khyzhun, A.K. Sinelnichenko, C.V. Ramana, Surface crystallography and electronic structure of potassium yttrium tungstate, J. Appl. Phys. 104 (2008), 033518.
- [56] J.C. Dupin, D. Gonbeau, P. Vinater, A. Levasseur, Systematic XPS studies of metal oxides, hydroxides and peroxides, Phys. Chem. Chem. Phys. 2 (2000) 1319–1324.
- [57] H. Perron, J. Vandenborre, C. Domain, R. Drot, J. Roques, E. Simoni, J.J. Ehrhardt, H. Catalette, Combined investigation of water sorption on TiO₂ rutile (1 1 0) single crystal face: XPS vs. Periodic DFT, Surf. Sci. 601 (2007) 518–527.
- [58] A. Trinchi, S. Kaciulis, L. Pandolfi, M.K. Ghantasala, X.Y. Li, W. Wlodarski, S. Viticoli, E. Comini, S. Sberveglieri, Characterization of Ga₂O₃-based MRISiC hydrogen gas sensors, Sens. Actuators, B 103 (2004) 129–135.
- [59] N. Syed, A. Zavabeti, Md Mohiuddin, B. Zhang, Y. Wang, R.S. Datta, P. Atkin, B. J. Carey, C. Tan, J. van Embden, A.S.R. Chesman, J.Z. Ou, T. Daeneke, K. Kalantar-Zadeh, Sonication-assisted synthesis of gallium oxide suspensions featuring trap state absorption: test of photochemistry, Adv. Funct. Mater. 27 (2017), 1702295.
- [60] W. Zhang, J.Z. Ou, S.Y. Tang, V. Sivan, D.D. Yao, K. Latham, K. Khoshmanesh, A. Mitchell, A.P. O'Mullane, K. Kalantar-Zadeh, Liquid metal/metal oxide frameworks, Adv. Funct. Mater. 24 (2014) 3799.
- [61] A.P. Grosvenor, B.A. Kobe, M.C. Biesinger, N.S. McIntyre, Investigation of multiplet splitting of Fe 2p XPS spectra and bonding in iron compounds, Surf. Interface Anal. 36 (2004) 1564–1574.
- [62] S. Sasikala, M. Ramalakshmi, K. Min, P. Shakkthivel, Facile biosurfactant-assisted biocompatible α-Fe₂O₃ nanorods and nanospheres synthesis, magneto physicochemical characteristics and their enhanced biomolecules sensing ability, RSC Adv. 6 (2016) 77133–77142.
- [63] Y. Gao, Y.J. Kim, S.A. Chambers, G. Bai, Synthesis of epitaxial films of Fe3O4 and α-Fe2O3 with various low-index orientations by oxygen-plasma-assisted molecular beam epitaxy, J. Vac. Sci. Technol. A 15 (1997) 332.
- [64] T. Fujii, F.M.F. de Groot, G.A. Sawatzky, F.C. Voogt, T. Hibma, K. Okada, In situ XPS analysis of various iron oxide films grown by NO2-assisted molecular-beam epitaxy, Phys. Rev. B 59 (1999) 3195–3202.
- [65] S. Jain, A.O. Adeyeye, S.Y. Chan, C.B. Boothroyd, Interface properties of iron oxide films, J. Phys. D Appl. Phys. 37 (2004) 2720–2725.

- [66] C.S. Kuivila, J.B. Butt, P.C. Stair, Characterization of surface species on iron synthesis catalysts by X-ray photoelectron spectroscopy, Appl. Surf. Sci. 32 (1988) 99–121.
- [67] V. Stambouli, C. Palacio, H.J. Mathieu, D. Landolt, Comparison of in-situ low-pressure oxidation of pure iron at room temperature in O2 and in O2/H2O mixtures using XPS, Appl. Surf. Sci. 70–71 (1993) 240–244.
- [68] J.S. Corneille, W. He, D.W. Goodman, Preparation and characterization of ultrathin iron oxide films on a Mo(100) surface, Appl. Surf. Sci. 338 (1995) 211–224.
- [69] M. Saleem, M.F. Al-Kuhaili, S.M.A. Durrani, I.A. Bakhtiari, Characterization of nanocrystalline α-Fe2O3 thin films grown by reactive evaporation and oxidation of iron, Phys. Scripta 85 (2012), 055802.
- [70] D.A. Armitage, D.M. Grant, Characterisation of surface modified nickel titanium alloys, Mater. Sci. Eng., A 349 (2003) 89–97.
- [71] C.C. Massaro, P. Rotolo, F. De Riccardis, E. Milella, A. Napoli, M. Wieland, M. Textor, N.D. Spencer, D.M. Brunette, Comparative investigation of the surface properties of commercial titanium dental implants. Part I: chemical composition, J. Mater. Sci. Mater. Med. 13 (2002) 535–548.
- [72] J.P. Schreckenbach, G. Marx, F. Schlottig, M. Textor, N.D. Spencer, Characterization of anodic spark-converted titanium surfaces for biomedical applications, J. Mater. Sci. Mater. Med. 10 (1999) 453–457.
- [73] L.Q. Wang, K.F. Ferris, A.N. Shultz, D.R. Baer, M.H. Engelhard, Interactions of HCOOH with stoichiometric and defective TiO₂(110) surfaces, Surf. Sci. 380 (1997) 352–364.
- [74] S. Sodergren, H. Siegbahn, H. Rensmo, H. Lindstrom, A. Hagfeldt, S.-E. Lindquist, Lithium intercalation in nanoporous anatase TiO2 studied with XPS, J. Phys. Chem. B 101 (1997) 3087–3090.
- [75] R. Gupta, S. Sen, Calculation of multiplet structure of core p-vacancy levels, Phys. Rev. B 12 (1975) 15–22.
- [76] S. Manandhar, C.V. Ramana, Direct, functional relationship between structural and optical properties in titanium-incorporated gallium oxide nanocrystalline thin films, Appl. Phys. Lett. 110 (2017), 061902.
- [77] A. Katrib, F. Hemming, P. Wehrer, L. Hilaire, G. Maire, The multi-surface structure and catalytic properties of partially reduced WO3, WO2 and WC+O2 or W+O2 as characterized by XPS, J. Electron. Spectrosc. Relat. Phenom. 76 (1995) 195–200.
- [78] F.Y. Xie, L. Gong, X. Liu, T. Tao, W.H. Zhang, S.H. Chen, H. Meng, J. Chen, XPS studies on surface reduction of tungsten oxide nanowire film by Ar⁺ bombardment, J. Electron. Spectrosc. Relat. Phenom. 185 (2012) 112–118.
- [79] P. Charton, L. Gengembre, P. Armand, TeO₂–WO₃ glasses: infrared, XPS and XANES structural characterizations, J. Solid State Chem. 168 (2002) 175–183.